Supporting Information for "Modeling the observed tropospheric BrO background: Importance of multiphase chemistry and implications for ozone, OH, and mercury"

J. A. Schmidt,[1,2] D. J. Jacob,[1,3] H. M. Horowitz,[3] L. Hu,[1] T. Sherwen,[4] M. J. Evans,[4] Q. Liang,[5] R. M. Suleiman,[6] D. E. Oram,[7] M. Le Breton,[8] C. J. Percival,[8] S. Wang,[9,10,11] B. Dix,[10] and R. Volkamer,[10,11]

Corresponding author: J. A. Schmidt, Department of Chemistry, Copenhagen University, Universitetsparken 5, DK-2100 Copenhagen O, Denmark. (schmidt@chem.ku.dk)

[1]Harvard University, School of Engineering and Applied Sciences, 29 Oxford St., Cambridge, MA 02138, USA

[2]University of Copenhagen, Department of Chemistry, Universitetsparken 5, Copenhagen, DK-2100, Denmark

[3]Harvard University, Department of Earth and Planetary Sciences, 20 Oxford St., Cambridge, MA 02138, USA

[4]Wolfson Atmospheric Chemistry Laboratories (WACL), Department of

Contents of this file

1. Introduction

Chemistry, University of York, York, YO10 5DD, UK

[5]NASA Goddard Space Flight Center, Laboratory for Atmospheric Chemistry and Dynamics, Greenbelt, MD 20771, USA

[6]Harvard Smithsonian Center for Astrophysics, 60 Garden St., Cambridge, MA 02138, USA

[7]Centre for Oceanography and Atmospheric Science, National Centre for Atmospheric Science, University of East Anglia, Norwich, NR4 7TJ, UK.

[8]The Centre for Atmospheric Science, School of Earth, Atmospheric and Environmental Sciences, University of Manchester, Brunswick St., Manchester, M13 9PL, UK

[9]Department of Chemistry, University of Michigan, 930 N. University Ave., Ann Arbor, MI 48109, USA

2. Figures S1 to S9

3. Tables S1 to S2

Introduction Figure S1 shows selected bromomethanes observed during CARIBIC, HIPPO (1–5) and TORERO aircraft campaigns compared to model output along the aircraft flight trajectories. The data is shown as mean vertical profiles. The model $CHBr_3$ and CH_2Br_2 emissions are based inventories of *Liang et al.* [2010]. The modeled $CHBr_3$ mixing ratios agree well with observations at all latitudes indicating that the balance between sources and sinks is consistent with reality. The modeled CH_2Br_2 mixing ratios agree well with CARIBIC and TORERO campaign observations, but are about 10% lower than HIPPO campaign observations in the PBL and mid troposphere indicating that the modeled CH_2Br_2 emission is slightly underestimated over the Pacific. *Parrella et al.* [2012] compared simulated $CHBr_3$ and CH_2Br_2 to TRACE-P, INTEX-B and ARCTAS campaign data and found similar good agreement between model and observations. The modelled CH_3Br mixing ratio agree well with observations from the HIPPO campaign. CH_3Br in GEOS-Chem is prescribed in the PBL to values of 6.7 ppt and 8.5 ppt in the S. and

[10]Department of Chemistry and
Biochemistry, University of Colorado,
Boulder, CO 80309, USA

[11]Cooperative Institute for Research in
Environmental Sciences, University of
Colorado, Boulder, CO 80309, USA

N. Hemisphere, respectively, which are similar to the NOAA and AGAGE network observed values in 2007 [*Montzka et al.*, 2010]. CH_3Br is minor contributor the tropospheric bromine budget and the observed errors in model CH_3Br only have very minor effect on tropospheric Br_y. Other brominated VOCs are not anticipated to contribute significantly to the tropospheric Br_y budget. Overall, we find that the bromocarbon source is well constrained.

Figure S2 shows the fraction multi-phase bromide cycling taking place through reactions with HOBr, $ClNO_3$ and O_3, respectively. HOBr is the dominant oxidant throughout the troposphere except in the upper tropical and subtropical troposphere where oxidation by ozone dominates. Bromide oxidation by $ClNO_3$ is most significant in the Northern Hemisphere over continental regions.

Figure S3 shows rate ratios for formation and removal of BrO, HOBr and $BrNO_3$. Figure S4 show the zonal mean BrO to BrO_x ratio. The partitioning of BrO_x between Br and BrO is controlled by BrO photolysis and the ozone + Br reaction. BrO photolysis in the lower troposphere is fastest in the tropics around noon peaking at a value of ~ 0.05 s^{-1}. In these areas Br would be the dominant form BrO_x if the ozone is less than 2-3 ppb.

The left panel of Fig. S5 shows the BrO relative difference between the standard simulation and a simulation with no stratospheric Br_y which approximates the fractionation of tropospheric BrO derived from input of stratospheric Br_y. The analysis suggest that input of stratospheric Br_y is the main contributor to BrO in the upper troposphere. The stratospheric source (flux) of Br_y to the troposphere is an order of magnitude smaller than the source from photochemical degradation of bromomethanes [*Parrella et al.*, 2012], but since stratospheric Br_y enters the upper troposphere where the lifetime of inorganic bromine is

longer due to limited wet deposition, this source gives a larger contribution to the tropospheric Br_y (and BrO) abundance. The right panel of Fig. S5 shows the change in ozone between the two simulations. We find that tropospheric ozone loss from Br_y originating from the stratosphere lowers ozone by < 1 ppb in the tropical MBL and up to 4 ppb in the extratropical upper troposphere.

Figure S6 (left panel) shows annual average ozone chemical production and change in production due to halogen chemistry. The right panel shows the ozone chemical lifetime and change in lifetime due to halogen chemistry.

A subset of the TORERO BrO observations were presented by *Volkamer et al.* [2015] and *Wang et al.* [2015] focusing on 6 flights that sampled the pristine free troposphere. Figure S7 compares model results the subsets of the full dataset.

Figure S8 shows the annual mean distribution of Br_y and BrO from the simulation including dehalogenation of acidic SSA (simulation B). Figure S9 shows the mean annual burden of SSA (below 1 km) and SSA bromide enhancement factor. A value of 0.5 indicate that the bromide content is 50 % that of dry sea salt. Values larger than 1 indicate enhanced levels of bromide in the SSA.

Model ozone concetrations were benchmarked against 2688 ozone profiles recorded at 53 different sites. Tables S1 and S2 list position and number of profiles for each site.

References

Liang, Q., R. S. Stolarski, S. R. Kawa, J. E. Nielsen, A. R. Douglass, J. M. Rodriguez, D. R. Blake, E. L. Atlas, and L. E. Ott (2010), Finding the missing stratospheric Br_y: a global modeling study of $CHBr_3$ and $CH2Br_2$, *Atmos. Chem. Phys.*, *10*, 2269–2286,

doi:10.5194/acp-10-2269-2010.

Montzka, S. A., S. Reimann, A. Engel, K. Krger, S. O'Doherty, W. T. Sturges, D. R. Blake, M. Dorf, P. Fraser, L. Froidevaux, K. W. Jucks, K. Kreher, M. J. Kurylo, A. Mellouki, J. Miller, O.-J. Nielsen, V. L. Orkin, R. G. Prinn, R. Rhew, M. L. Santee, A. Stohl, and D. Verdonik (2010), Ozone-Depleting Substances (ODSs) and related chemicals, chapter 1 in scientific assessment of ozone depletion: 2010, Global Ozone Research and Monitoring Project-Report No. 52, 516 pp., World Meteorological Organization, Geneva, Switzerland.

Parrella, J. P., D. J. Jacob, Q. Liang, Y. Zhang, L. J. Mickley, B. Miller, M. J. Evans, X. Yang, J. A. Pyle, N. Theys, and M. Van Roozendael (2012), Tropospheric bromine chemistry: implications for present and pre-industrial ozone and mercury, *Atmos. Chem. Phys.*, *12*, 6723–6740, doi:10.5194/acp-12-6723-2012.

Volkamer, R., S. Baidar, T. L. Campos, S. Coburn, J. P. DiGangi, B. Dix, T. K. Koenig, I. Ortega, B. R. Pierce, M. Reeves, R. Sinreich, S. Wang, M. A. Zondlo, and P. A. Romashkin (2015), NO_2, H_2O, O_2-O_2 and aerosol extinction profiles in the tropics: Comparison with aircraft-/ship-based in situ and lidar measurements, *Atmos. Meas. Tech.*, *8*(1), 2121–2148, doi:10.5194/amt-8-2121-2015.

Wang, S., J. A. Schmidt, S. Baidar, S. Coburn, B. Dix, T. K. Koenig, E. Apel, D. Bowdalo, T. L. Campos, E. Eloranta, M. J. Evans, J. P. DiGangi, M. A. Zondlo, R.-S. Gao, J. A. Haggerty, S. R. Hall, R. S. Hornbrook, D. Jacob, B. Morley, B. Pierce, M. Reeves, P. Romashkin, A. ter Schure, and R. Volkamer (2015), Active and widespread halogen chemistry in the tropical and subtropical free troposphere, *Proc. Natl. Acad. Sci. USA*, doi:10.1073/pnas.1505142112.

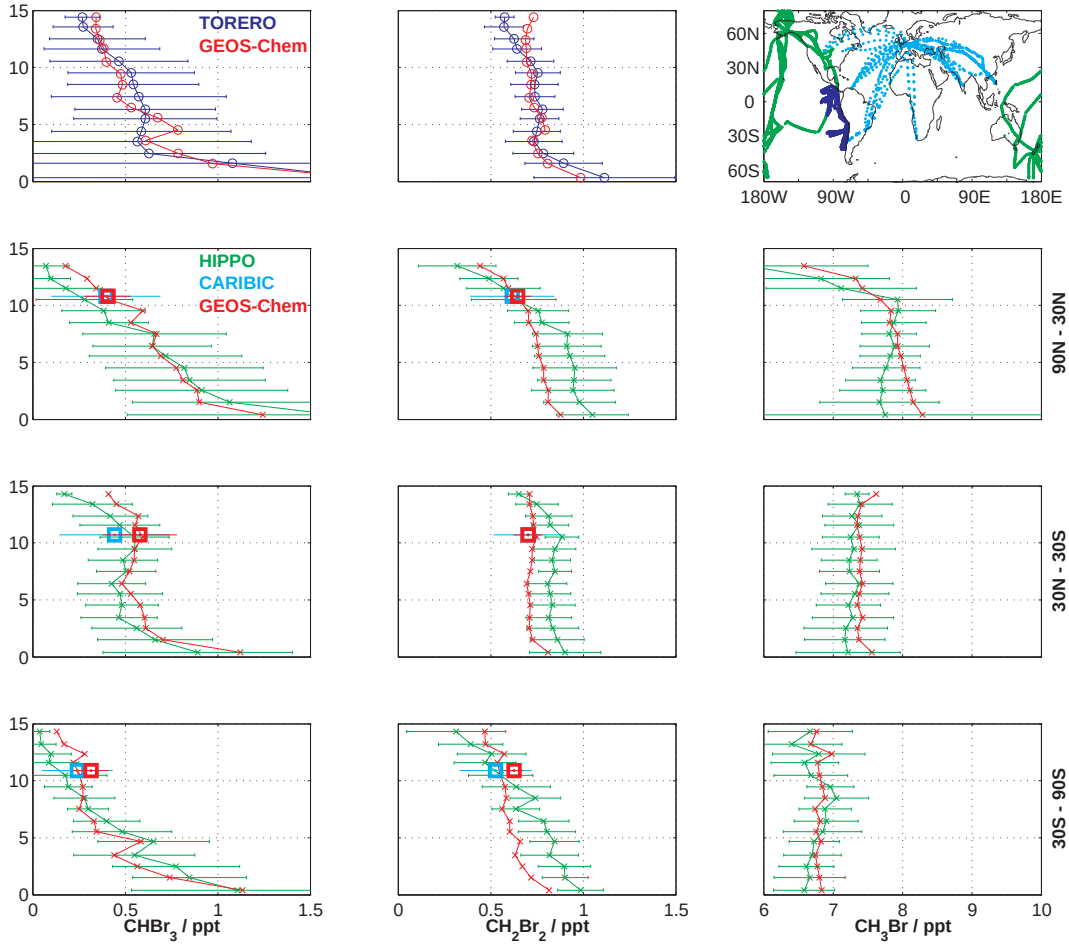

Figure S1. Observed and modeled bromocarbon mixing ratios. HIPPO and CARIBIC data is separated in 3 zonal bands. Bromocarbon vertical profiles for TORERO (blue) and HIPPO (green) campaigns are for 1 km wide bins and compared to corresponding model data (red). CARIBIC $CHBr_3$ and CH_2Br_2 data (cyan square) averaged between 8 and 12 km is compared to corresponding model data (red square). The error bars show 1 standard deviation. The flight paths of the three field campaigns are also shown.

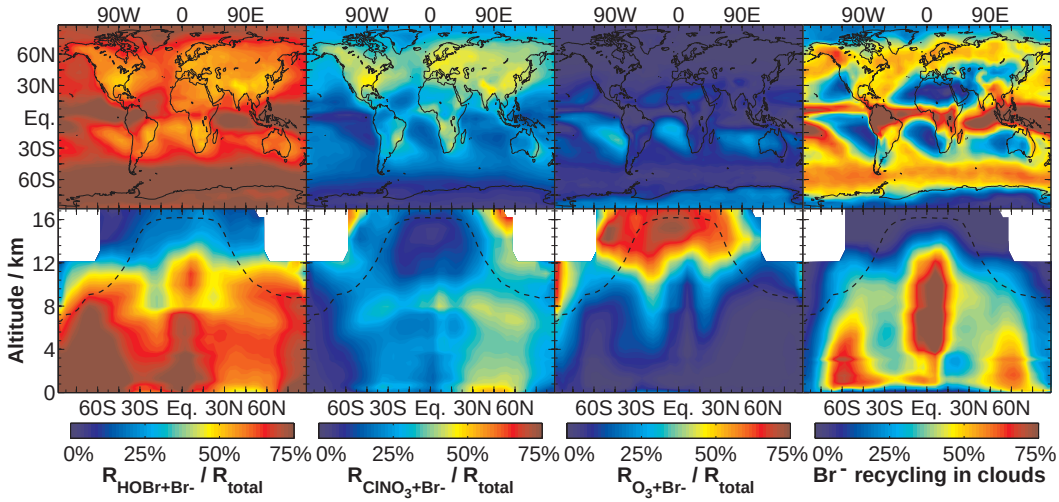

Figure S2. Fraction multi-phase bromide cycling by 3 different oxidants and by multiphase chemistry in clouds. R_{total} is equal to $R_{\mathrm{HOBr+Br-}} + R_{\mathrm{ClNO_3+Br-}} + R_{\mathrm{O_3+Br-}}$

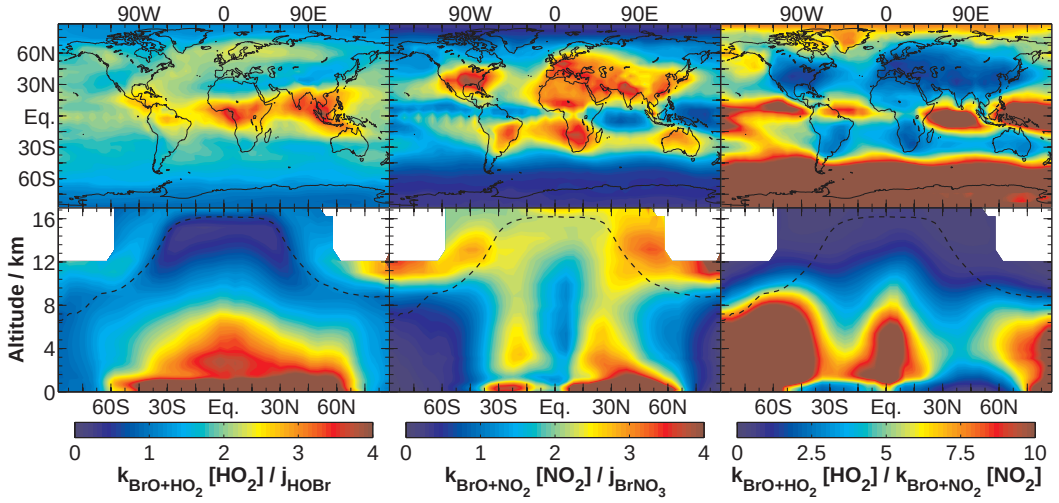

Figure S3. Rate ratios

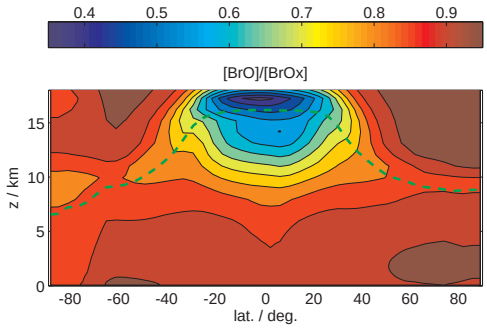

Figure S4. Zonal mean BrO to BrO_x ratio.

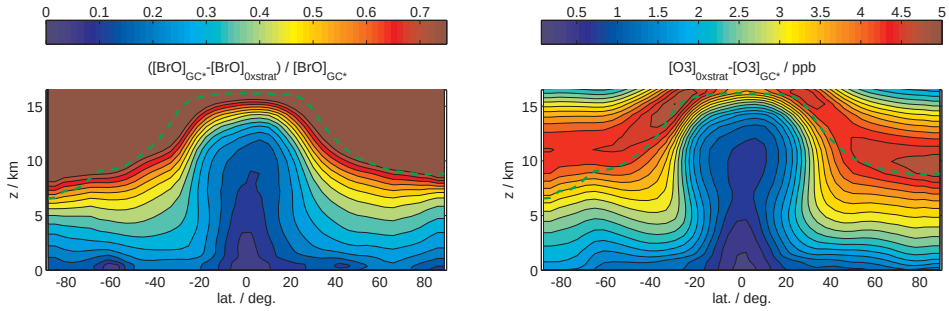

Figure S5. Left panel: Relative difference in BrO between current simulation ($[BrO]_{GC*}$) and a simulation with no Br_y in the stratosphere ($[BrO]_{0\times strat}$). Right panel: Difference in ozone between current simulation and a simulation with no Br_y in the stratosphere.

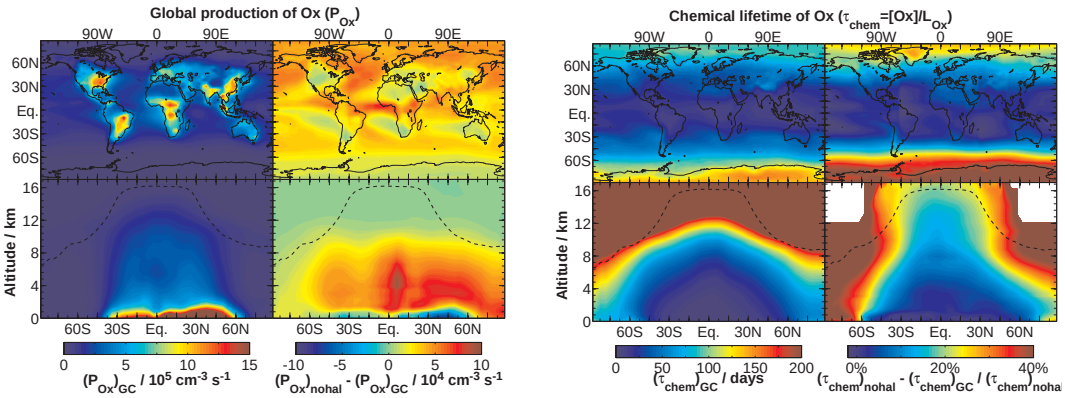

Figure S6. Left: Annual average ozone chemical production and change in production due to halogen chemistry. Right: Ozone chemical lifetime and change in lifetime due to halogen chemistry.

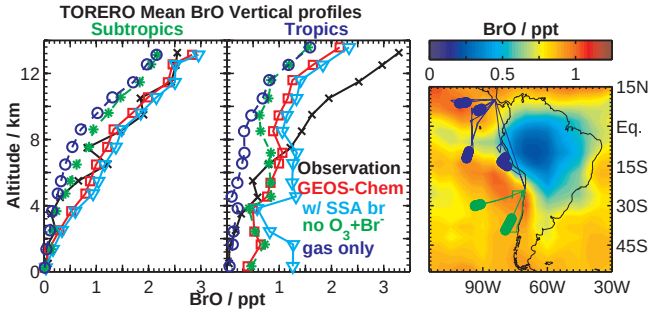

Figure S7. Mean vertical profiles of BrO concentration over the Southeast Pacific. A subset of daytime aircraft observations from the TORERO campaign (January-February 2012) presented in *Volkamer et al.* [2015] and *Wang et al.* [2015] are compared to GEOS-Chem values sampled along the 6 flight tracks of the subset. Also shown are results from model sensitivity simulations with SSA debromination, without the aqueous phase O_3+Br^- reaction, and without multiphase halogen chemistry (gas-phase chemistry only). The right panel shows the TORERO flight tracks superimposed on the model distribution of daytime tropospheric mean BrO mixing ratios for the flight period.

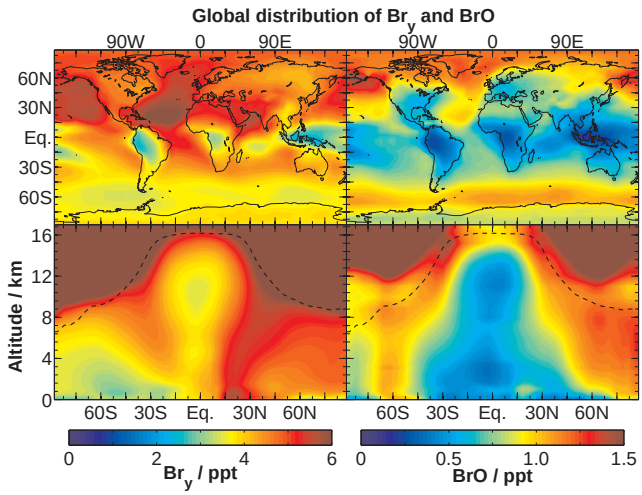

Figure S8. Annual mean global distributions of tropospheric Br_y and BrO from simulation including SSA dehalogenation. Multiply BrO concentrations by a factor of 2 for daytime values (this approximation is not valid at high latitudes during winter and summer). Top panels: mean tropospheric mixing ratios. Bottom panels: zonal mean mixing ratios as a function of altitude and latitude. The tropopause is shown as dashed line.

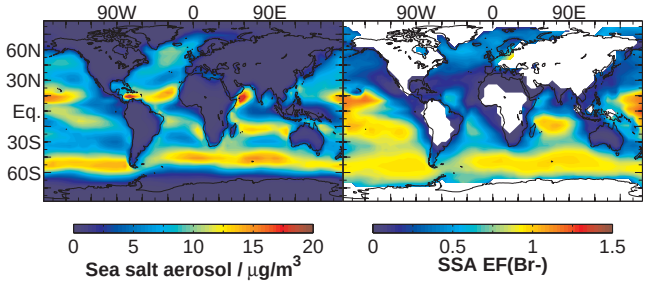

Figure S9. Left: Annual mean global burden of sea salt aerosol from 0 to 1 km. Right: SSA bromide depletion: A value of 0.5 (1.5) indicate that the bromide content is 50 % (150 %) that of sea salt.

Table S1. Ozone sonde information. Site position and number of samples (N_s).

Site name	Lat.	Lon.	N_s	Site name	Lat.	Lon.	N_s
Alert	83	-62	68	Eureka	80	-86	88
Ny-Aalesund	79	12	90	Resolute	75	-95	49
Summit	73	-38	45	Lerwick	60	-1	55
Churchill	59	-94	52	Stony Plain	54	-114	48
Goose Bay	53	-60	54	Legionowo	52	21	40
Lindenberg	52	14	72	De Bilt	52	5	52
Valentia Observatory	52	-10	32	Uccle	51	4	141
Bratts Lake	50	-105	35	Praha	50	14	47
Kelowna	50	-119	46	Hohenpeissenberg	48	11	127
Payerne	46	7	157	Egbert	44	-80	45
Yarmouth	44	-66	44	Narragansett	41	-71	42
Trinidad Head	41	-124	47	Barajas	40	-4	36
Boulder	40	-105	53	Ankara	40	33	21
Wallops Island	38	-75	50	Huntsville	35	-87	56
Isfahan	33	52	6	Hong Kong	22	114	44

Table S2. Ozone sonde information (Continued). Site position and number of samples (N_s).

Site name	Lat.	Lon.	N_s	Site name	Lat.	Lon.	N_s
Hanoi	21	106	28	Hilo	19	-155	94
Heredia	10	-84	1	Alajuela	10	-84	42
Cotonou	6	2	6	Paramaribo	6	-55	55
Sepang Airport	3	102	44	San Cristobal	-1	-90	34
Nairobi	-1	37	59	Natal	-5	-35	24
Watukosek (Java)	-8	113	15	Ascension Island	-8	-14	44
Samoa	-14	-171	93	Suva	-18	178	8
La Reunion	-21	55	15	Irene	-26	28	20
Broadmeadows	-38	145	44	Lauder	-45	170	39
Macquarie Island	-55	159	45	Marambio	-64	-57	70
Davis	-69	78	29	Neumayer	-71	-8	67
South Pole	-90	169	70				